

## Corrosion Inhibition of Pipeline Steel X-70 in Sour Brine by an Imidazoline Derivative under Flow Assisted Conditions

M. Díaz-Cruz<sup>1,\*</sup>, M. A. Domínguez-Aguilar<sup>2</sup>, A. Cervantes-Tobón<sup>1</sup>, B. Castro-Domínguez<sup>3</sup>,  
F. Jiménez-Cruz<sup>2</sup>, M.T. Fuentes-Romero<sup>4</sup>.

<sup>1</sup> Instituto Politécnico Nacional, Departamento de Ingeniería Metalúrgica, IPN-ESIQIE, U.P. Adolfo López Mateos, Zacatenco, C.P. 07738, México, D.F., México.

<sup>2</sup> Instituto Mexicano del Petróleo, Laboratorio de Producción de Hidrocarburos y Control de la Corrosión, Eje Central Norte Lázaro Cárdenas 152, Col. San Bartolo Atepehuacan, C.P. 07730, México D.F., México.

<sup>3</sup> Worcester Polytechnic Institute, Center for Inorganic Membrane Studies, Department of Chemical Engineering, Worcester Massachusetts, WA 01609, US.

<sup>4</sup> Universidad Tecnológica Fidel Velázquez, Departamento de Nanotecnología, Av. Emiliano Zapata S/N, El Tráfico, 54400 Villa Nicolás Romero, Atizapán, Edo. De México, México

\*E-mail: [mdiazc@ipn.mx](mailto:mdiazc@ipn.mx), [neladiaz1346@gmail.com](mailto:neladiaz1346@gmail.com)

Received: 25 April 2016 / Accepted: 10 January 2017 / Published: 12 July 2017

---

The corrosion behavior of a pipeline steel API 5L X-70 was tested under flow assisted conditions in a sour brine solution containing kerosene in the presence of an imidazoline derivative. Inhibitor film provided efficiencies in the range of 70-99% at 200 ppm with initial corrosion rates in the range of 125-134 mpy (3.2-3.4 mm/y). In the absence of inhibitor, chemical species of cubic maghemite (Fe<sub>2</sub>O<sub>3</sub>) predominated with an apparent decrease in orthorhombic marcasite (FeS<sub>2</sub>) on the steel surface when angle was increased from 30° to 90°. In the presence of inhibitor, maghemite (Fe<sub>2</sub>O<sub>3</sub>) and marcasite (FeS<sub>2</sub>) prevailed as a mixture of oxides and sulfides at the impingement angles. Mackinawite appeared with and without the presence of corrosion inhibitor at every angle tested. As flow rate and angle are increased, inhibitor efficiency decreased due to partial film formation. Imidazoline derivative is efficient albeit a periodic replenishment is required after a 3-4 hour period. DFT molecular simulation of imidazoline derivative emphasized nitrogen polarity and capability of interacting with another molecular species.

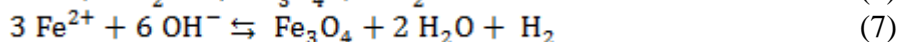
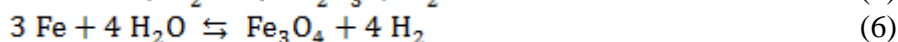
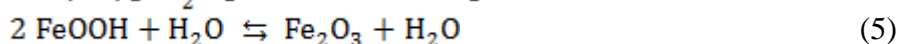
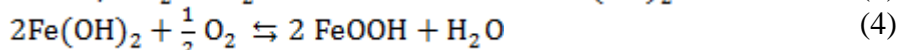
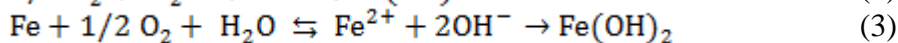
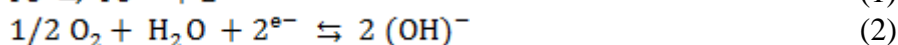
---

**Keywords:** Flow assisted corrosion, sour brine, jet impingement, API X-70.

### 1. INTRODUCTION

The internal corrosion of pipelines is a serious problem in the oil & gas industry as it affects mechanical integrity of chemical plant, equipment and piping systems. The interaction of a fluid in

motion with pipe wall leads to flow assisted corrosion (FAC). This type of corrosion is aqueous and generally occurs in carbon steels in liquid and liquid/vapor mixtures but not in dry gases. FAC takes place on the boundary layer of the metallic surface where the anodic dissolution of iron produces  $\text{Fe}^{2+}$  and  $\text{Fe}(\text{OH})_2$ . Iron hydroxide inhibits corrosion after certain condensation reactions then this layer is converted into magnetite (black colored oxide  $\text{Fe}_3\text{O}_4$ ), which may reach a thickness of 15-25  $\mu\text{m}$  in the temperature range of 150-280  $^\circ\text{C}$  and it can be very thin ( $< 1 \mu\text{m}$ ) below 150  $^\circ\text{C}$ . Under laminar flow conditions, this oxide is protective and its growth is balanced with its dissolution in flowing water. However, under turbulence resulting from local geometries, the dissolved ferrous ions are more rapidly removed from the surface and corrosion occurs [1, 2]. The rate of this process depends on the rate of mass transfer of ferrous ions from the metal surface to the bulk of flowing water [3], which in turns depends on hydrodynamics, environmental and metallurgical factors. The basic reactions of FAC included, iron oxidation and water reduction (1, 2) to form iron hydroxide (3) and oxyhydroxides (4), with hematite in the outer layer (5) and magnetite (6, 7) at the inner layer of oxide [4-6], other chemical species can be formed depending on the testing environment [7]:



FAC has an important effect on vessels, process equipment and a large number of components as it produces turbulence and commonly a slug flow pattern of liquid and gas, this turbulence removes the protective corrosion products to produce a wall thinning that reduces mechanical strength and loss of containment. FAC is commonplace in the nuclear power plant, electric and chemical process industries [8-11], in which fluid flow enhances corrosion rates by an accelerated mass transfer of reactants and corrosion products disrupt the passive film by a rubbing process. FAC can be influenced by shear stress, flow separation, turbulence and characteristics of the dispersed phase. Furthermore, in industrial applications FAC has been identified as one of the main degradation mechanisms that demands for frequent maintenance of equipment and piping that transport fluids so as to preserve mechanical integrity [12].

Carbon steels are widely used in the oil and gas industry despite their corrosion resistance is limited. These materials are preferred to others because of economic considerations and the fact that its corrosion usually leads to general attack. The API 5L pipe steel is a low carbon steel, which is used for the fabrication of transmission pipelines [13, 14]. The development of technology for high strength pipeline steel such as X-80, X-100 and X-120 through thermo-mechanical process allowed a reduction in wall thickness and sometimes an improvement in corrosion resistance [15, 16]. However, the API 5L pipe is still susceptible to aqueous corrosion so inhibitor addition is a frequent corrosion control measurement.

Imidazolines inhibitors have been on use for more than forty five years with an improved performance [17, 18]. The importance and usefulness of oleic imidazoline in the oil and gas pipelines has been studied in detail by several researchers [19-21]. Most of these commercial inhibitors have organic molecules that are adsorbed onto the metal surface to form a protective film. Imidazolines are the most extensively used inhibitors to mitigate CO<sub>2</sub> corrosion [22-25]. Likewise, they are also useful in controlling corrosion by hydrogen sulfide in wet sour gas [26], crude oil [27, 28], oil water emulsions [29] sour brines [30], and drilling muds [31] as well as in environments with minor contents of water combining CO<sub>2</sub>/H<sub>2</sub>S in the presence of chlorides [32].

This paper aims to investigate what chemical species are deposited on the metallic surface of a pipeline steel API 5L X-70 before and after the addition of a corrosion inhibitor (CI) under flow assisted conditions. This consisted in varying mass flow rate of an aqueous brine solution saturated with H<sub>2</sub>S and changing jet angle of impingement on the metallic coupons. The composition and morphology of the chemical species deposited in the form of corrosion products/inhibitor films contribute largely in determining corrosion rate and inhibitor efficiency as they determine the degree of porosity and adhesion to the metallic substrate and consequently their tendency to cracking and dissolution. X-ray diffraction and electronic microscopy aided in determining how corrosion and inhibition interact on carbon steel microstructure.

## 2. EXPERIMENTAL PROCEDURE

### 2.1 Materials and equipment

Samples of pipeline steel API 5L-X70 were cut and machined into coupons of 1 cm x 0.5 cm x 1 cm in order to provide a working area of 0.5 cm<sup>2</sup>. Three coupons of similar dimensions were wet abraded with emery paper, mounted in resin and welded to electric wires for connection to electrochemical equipment. The coupon set is placed in the test chamber made of clear acrylic in which a free jet impingement device is introduced. The chamber is provided with a tilted plate at the bottom for rapid fluid drain and recovery for appropriate disposal; inlet and outlet connections as well as movable plate, where metallic coupons are placed at the testing angles of 30°, 60° and 90°. Electrolyte consisted in a brine solution prepared according to the following composition (g/L): NaCl (106.57); CaCl<sub>2</sub>\*2 H<sub>2</sub>O (4.47); MgCl<sub>2</sub>\*6H<sub>2</sub>O (2.06) saturated with hydrogen sulfide to pH 4, besides 10 % of kerosene as organic phase [33]. Sour brine is recirculated by a centrifugal pump and stored in a polyethylene tank with capacity of 100 L. The electrolyte is fed from the storage tank to the jet impingement and from there to the metallic coupon surfaces located in the testing chamber.

### 2.2. Corrosion rate measurements

Linear polarization resistance measurements were performed on the previously resin mounted steel samples electrode for jet impingement tests. The jet impingement chamber and the electrochemical cell consisted of an arrangement of two electrodes made of the same carbon steel material and a reference electrode of SS 316L [34], which allowed carrying out testing in a

manageable scheme though it introduced an error of around  $\pm 10\%$  in corrosion rate measurements. Experimental tests were controlled by means of the POWER SUIT software in a potentiostat-galvanostat made by Princeton Applied Research model 263A. The polarization scans were carried out on the steel at  $\pm 20$  mV vs. the open circuit potential (OCP) at a rate of 0.166 mV/s in a brine containing 10% kerosene and 1383 ppm of H<sub>2</sub>S. Corrosion rates were determined from polarization resistance measurements according to the Stern-Geary's equation (8) by means the  $R_p$  (ohm-cm<sup>2</sup>) provided as a function of flow rate (8 and 18 l/min) and testing time (1-8 hours). Procedure consisted in calculating current density  $J_{\text{corr}}$  and corrosion rate (9) as follows:

$$J_{\text{corr}} = \frac{B}{R_p} = x = \frac{\beta_a \times \beta_c}{2.3 \times R_p \times (\beta_a \times \beta_c)} \quad (8)$$

$$\text{CR} = \frac{0.00327 \times J_{\text{corr}} (\mu\text{A}/\text{cm}^2) \times \text{EW}}{\rho (\text{g}/\text{cm}^3)} \quad (9)$$

where  $\beta_a$  and  $\beta_c$  are the anodic and cathodic Tafel constants; 0.00327 is a constant used for dimension and time conversion [35], EW is the equivalent weight of corroded iron (27.8 g/g mol) and  $\rho$  is steel density (7.8 g/cm<sup>3</sup>). In this study B is assumed to be 0.026 V; this data was taken from measurements performed at pH 4 [36] and whose slopes range within 60-120 mV/decade. The system under study stabilized itself at a roughly constant open circuit potential of -0.71 mV to -0.84 after about 60 minutes. Three tests were performed every hour to ensure measurement reliability. Inhibitor was added once every 8 hours at a constant dosage of 200 ppm. Potentiodynamic curves were performed  $\pm 250$  mV vs. OCP at a rate of 0.166 mV/s.

### 2.3. Surface characterization

Images of corroded surfaces and those after inhibitor addition were recorded in a scanning electron microscope (SEM) JEOL-JSM 6300. X-ray diffraction (XRD) was performed in a D8 Focus Bruker diffractometer with Cu K $\alpha$  radiation to determine the nature of chemical species deposited on metallic coupons as corrosion deposits and films by using the grazing incidence technique (GIXRD). X-ray scanning was performed within the range of 20° to 90° with a step width of 0.02°; further analysis of XRD spectra was carried out with the CreaFit 2.2 DRXW software.

### 2.4 Quantum chemical calculations

The molecular structure of the compound is schematically shown in Figure 1, this compound was studied by the DFT method, with an optimized geometry at B3LYP/6-31G\* level of theory [37]. For energy minimization a convergence limit was set at unity with 1 kcal/A mol as rms gradient. The professional software Spartan 02 [38] was employed for calculations including: HOMO and LUMO energies as well as Mulliken's electronegativity.

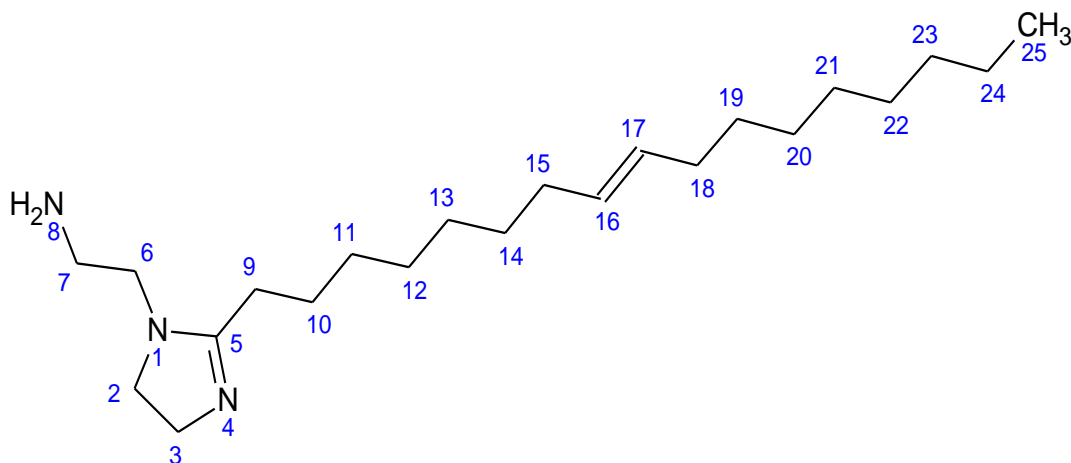


**Figure 1.** Molecular structure of 2-{2-[(8E)-heptadec-8-en-1-yl]-4,5-dihydro-1H-imidazol-1-yl}ethanamine

### 3. RESULTS AND DISCUSSION

#### 3.1. Chemical analysis and metallography

The chemical composition of the pipeline steel X-70 was determined by optical emission spectroscopy by spark discharge, whose elements in wt. % are as follows: C (0.24), Mn (1.081), Si (0.284), P (0.019), S (0.021), Cr (0.156), Cu (0.185), Ni (0.088) balance with Fe. Microstructure of steel X-70 (Figure 2) consisted of a uniform distribution of ferrite and lamellar pearlite in colonies distributed over a matrix of ferrite, which is typical of a normalized carbon steel.

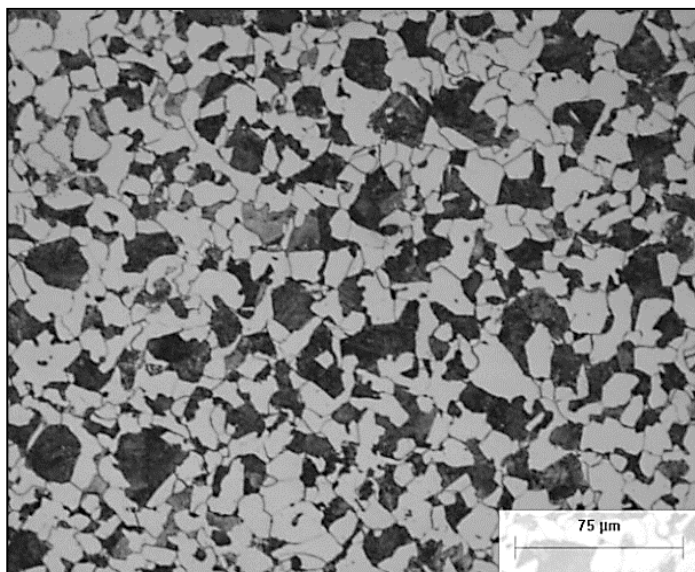


**Figure 2.** Microstructure of steel API 5L X-70 etched in 5% nital (500X) showing ferrite and pearlite in light and dark contrast, respectively.

3.2 Polarization scans

3.2.1 Corrosion rates as function of flow rate and impingement angles

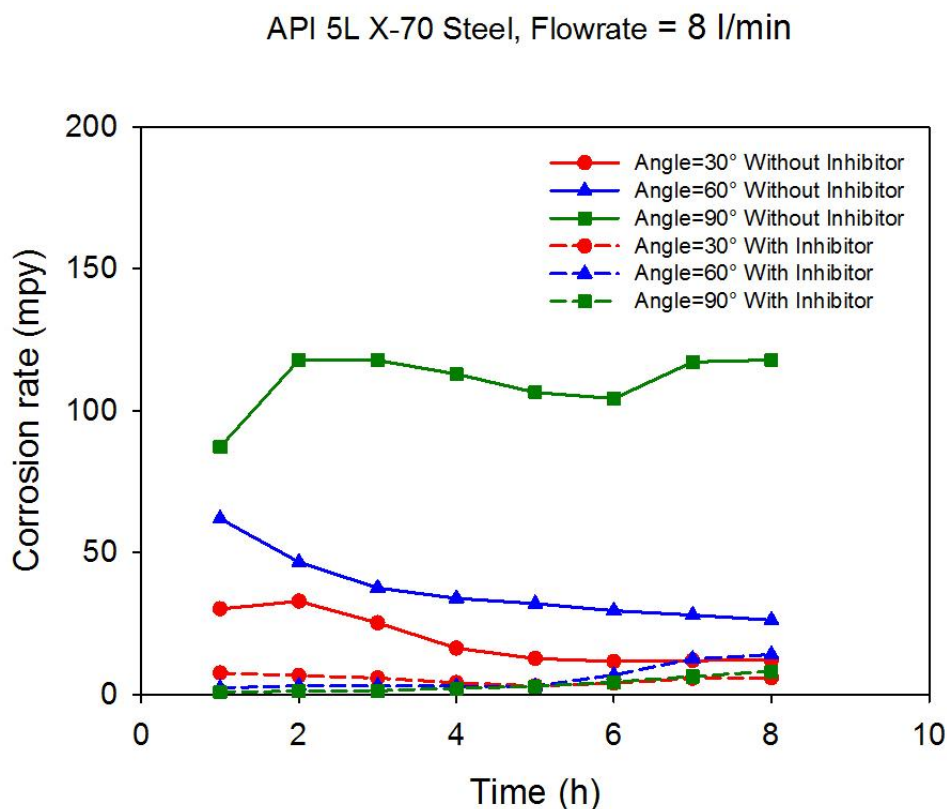


**Figure 3.** Corrosion rate of pipeline steel API X-70 for the impinging angles of 30°, 60° and 90° at a flow rate of 8 L/min with and without corrosion inhibitor for a testing time of 8 h.

Figure 3 shows the corrosion rate versus time for a flow rate of 8 l/min at the impingement angles of 30°, 60° and 90°. For testing without inhibitor, the highest corrosion rates were recorded in the coupon placed at 90° (~120 mpy), followed by that at 60° (~60 mpy) and 30° (~30 mpy). It is evident the effect of corrosion inhibitor on corrosion as it displaced curves down ca. ~10 mpy.

**Table 1.** Average corrosion rates at the testing conditions with and without corrosion inhibitor.

Testing conditions		*Corrosion rate (mpy)			
		Flow rate			
Impingement angle	Time (h)	8 L/min		18 L/min	
		V <sub>i</sub>	V <sub>f</sub>	V <sub>i</sub>	V <sub>f</sub>
30°	1	30	7.0	167	18.4
	8	12	5.8	70	30.5
60°	1	62	2.2	134	40.3
	8	26	14	67	46.6
90°	1	87	0.7	125	10.3
	8	118	8.0	86	56.8

\*V<sub>i</sub>/V<sub>f</sub>: corrosion rate in the absence and presence of 200 ppm inhibitor.

**Table 2.** Efficiency of CI as a function of time and flow rates of 8 l/min and 18 l/min.

Testing time (h)	8 L/min			18 L/min		
	30°	60°	90°	30°	60°	90°
1	75.2	96.4	99.2	88.9	69.9	92.0
2	80.1	93.6	99.1	88.3	71.9	94.6
3	77.3	92.2	98.9	83.7	80.4	93.3
4	75.1	91.7	98.2	81.2	31.8	92.1
5	76.8	91.3	97.4	92.0	9.6	69.6
6	67.0	77.1	95.9	88.5	24.2	60.2
7	53.5	55.7	94.7	81.3	12.1	50.3
8	51.8	46.5	93.2	56.2	30.3	34.1

In Tables 1 and 2, it can be observed that the initial corrosion rates before the addition of inhibitor were in the range of 30-118 mpy for 8 l/min, while at 18 l/min they reached 67-168 mpy. However, after inhibition they decreased to ~1-14 mpy (8 l/min) and ~6-57 mpy (18 l/min), respectively. At 8 l/min, CI efficiencies reached 75-99% and at 18 l/min were in the range of 70-95%. After 8 hours testing with CI and for both flow rates, the highest corrosion rates were obtained at 90° (~ 57 mpy), whilst at 60°/30°, they decreased to an average of 10 mpy.

API 5L X-70 Steel, Flowrate = 18 l/min

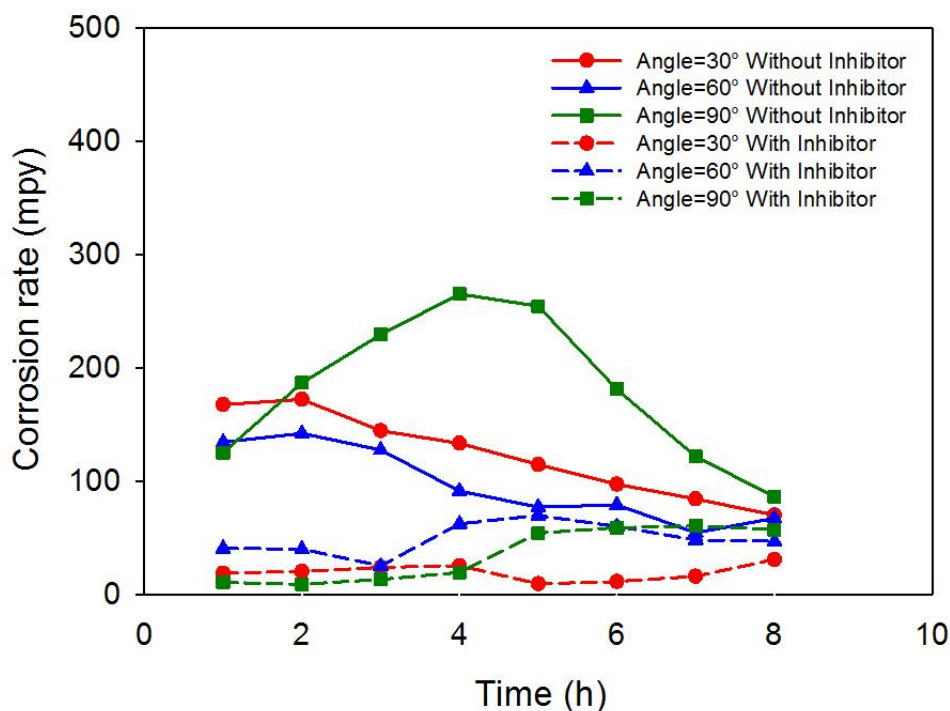


**Figure 4.** Corrosion rate of pipeline steel API X-70 for the impinging angles of 30°, 60° and 90° at a flow rate of 18 l/min with and without corrosion inhibitor for a testing time of 8 h.

Figure 4 shows the corrosion rate versus time for a flow rate of 18 l/min at angles of 30°, 60° and 90°. For testing without inhibitor, the highest corrosion rates were recorded again in the coupon set at 90° (~260 mpy), followed by that at 60° (~140 mpy) and 30° (~32 mpy). CI mitigated corrosion though its effect is for a period of three hours as a result of increased turbulence.

When imidazoline derivative was added, corrosion rates decreased for a period of 3-4 hours. CI proved to be highly efficient for the first hours. However, it is necessary to add another dose of CI after 4 hours at 8 l/min to maintain a low and constant corrosion rate, whereas at 18 l/min, CI addition is required after 3 hour of testing. At 8 l/min (Figure 2) corrosion rates were within 1-4 mpy for 4 hours then corrosion rate increased to roughly 10 mpy after 8 h. At 18 l/min (Figure 4), corrosion rates dropped within 5-20 mpy for the first 3 hours to increase to 6-48 mpy after 8 hours.

Figure 5 shows an example of the polarization scans performed at 18 l/min along with the electrochemical parameters (Table 3). Potentiodynamic curves showed the effect of corrosion inhibitor, which consisted in decreasing the open circuit potential towards more noble potentials along with a decrement in the current density as a result of film formation. The blank material of X-70 shows the same tendency when testing time increased from 0 to 4 hours though now because of the formation of corrosion products. The latter also occurred when 10 ppm of inhibitor was added, which is related to the arrests showed on the cathodic branch of the curve.

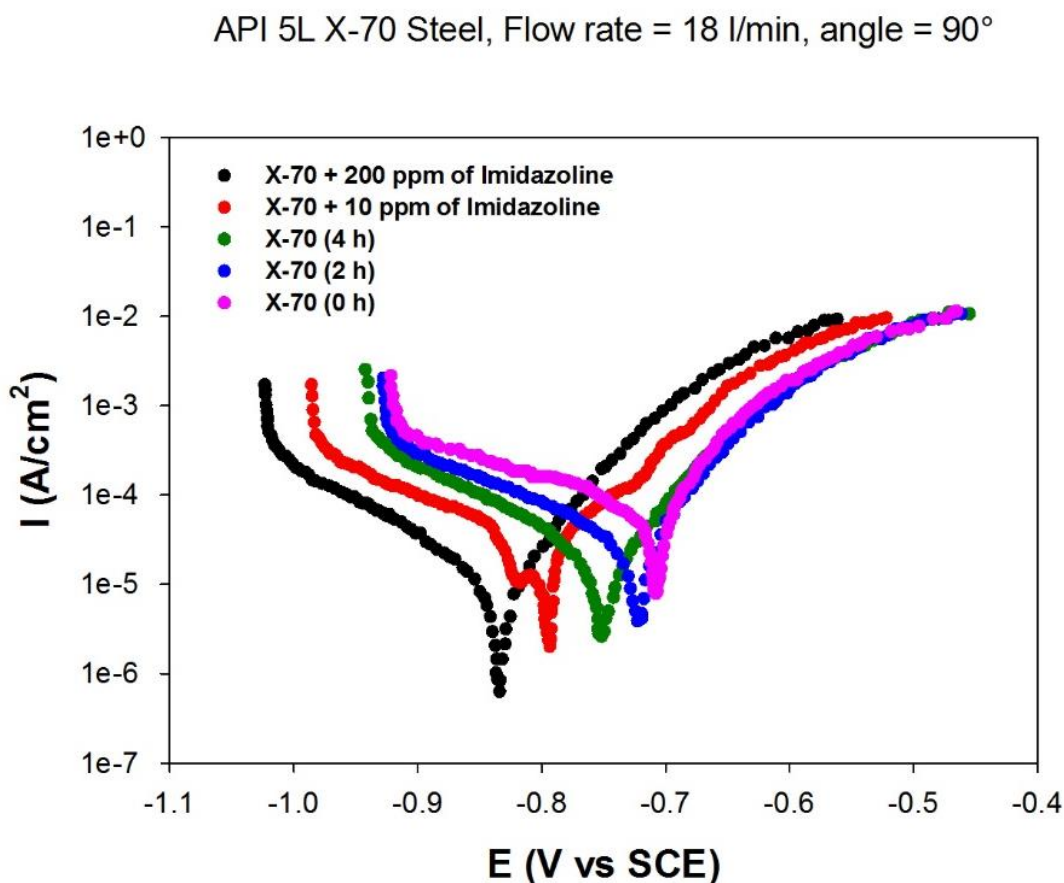


**Figure 5.** Polarization scans for X-70 coupons in sour brine at 18 l/min.

**Table 3.** Corrosion parameters in the absence/presence of CI at 18 l/min at 90°

Time (h)	E (mV)	$i_{\text{corr}}$ (A/cm <sup>2</sup> )	$R_p$ (ohm cm <sup>2</sup> )	$\beta_c$ (mV dec <sup>-1</sup> )	$\beta_a$ (mV dec <sup>-1</sup> )	$V_{\text{corr}}$ (mpy)
X-70, 0 h	-0.710	$2.3 \times 10^{-4}$	219	138	126	125
X-70, 2 h	-0.730	$1.9 \times 10^{-4}$	268	90	120	94
X-70, 4 h	-0.750	$1.2 \times 10^{-4}$	365	110	145	86
X-70 + 10 ppm, 1 h	-0.790	$6.4 \times 10^{-5}$	787	127	107	32
X-70 + 200 ppm, 1 h	-0.840	$2.7 \times 10^{-5}$	1490	131	157	10

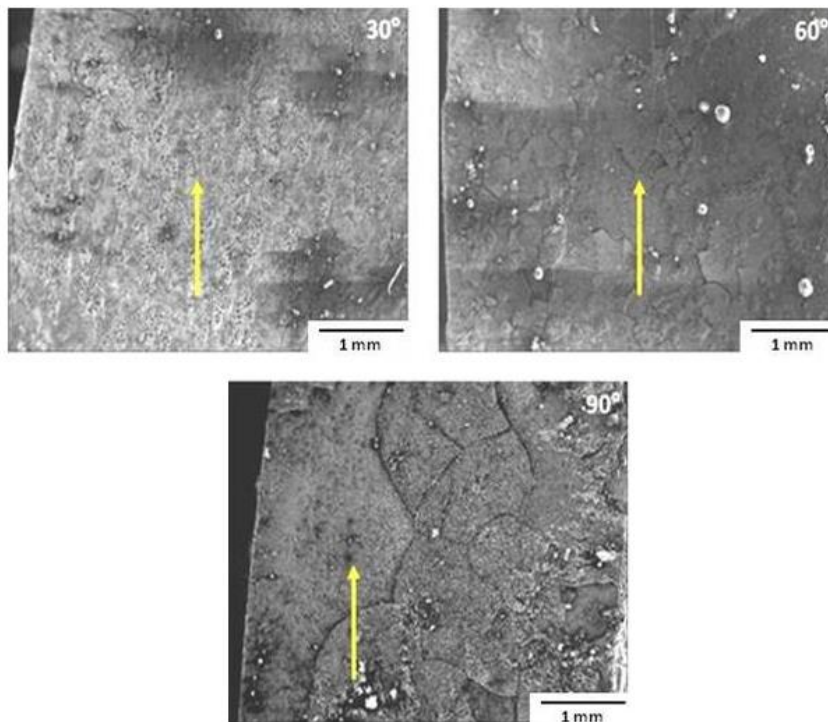
The corrosion inhibition efficiency of organic compounds, such as imidazolines, is strongly dependent on molecular adsorption on substrate surface. Adsorption depends on the nature and metallic surface condition, type of corrosive medium and chemical structure of inhibitor. Studies report [39, 40] that the adsorption of organic inhibitors mainly depends on some physicochemical properties of the molecule, related to its functional groups, steric effects and electronic density of donor atoms; adsorption is supposed to depend on the possible interaction of *p*-orbitals of the inhibitor with *d*-orbitals of the surface atoms, which induce greater adsorption of the inhibitor molecules onto the surface of carbon steel, leading to the formation of a corrosion protecting film [41]. However, under turbulent flow conditions inhibitor film can be removed from steel surface at some critical flow velocity [42], which indicates that shear stress can remove inhibitor layers and decrease their efficiency. In contrast, the shear stress to remove an imidazoline base inhibitor ranged within 50-100 MPa after atomic force measurement, which is much higher than the shear stress produced in high turbulence flow. In any case, corrosion phenomenon is still produced because of inhibitor film porosity and batches of film deposited on steel surface though inhibitor should add to maintain a steady state and mitigate corrosion rate [43].

### 3.3 SEM surface characterization

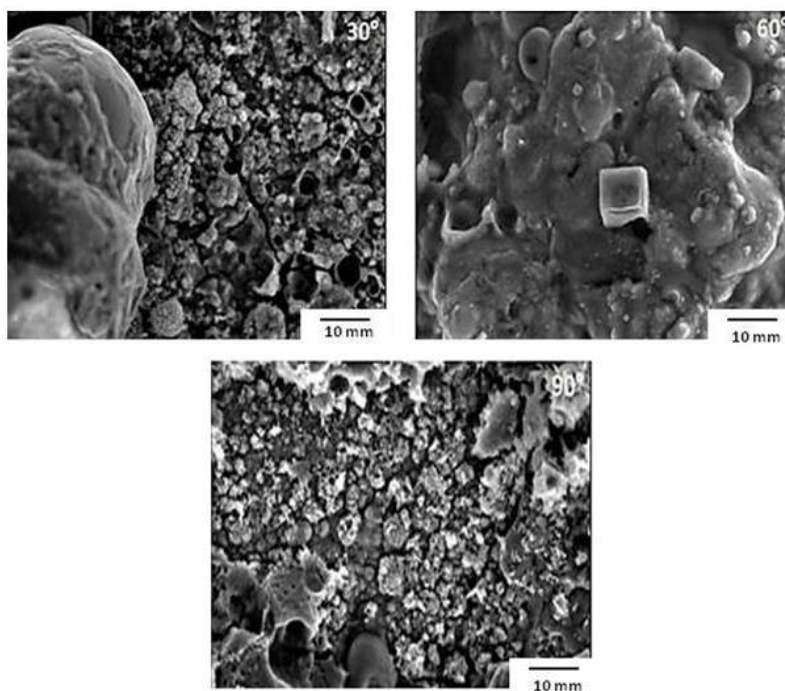
#### 3.3.1 SEM characterization at a flow rate of 18 l/min without inhibitor

Figure 6 shows the coupon surfaces after conducting the test at a flow rate of 18 l/min (2.36 m/s). It is noticed that flow rate promoted corrosion product removal and cracking in the layer of the corrosion products. The degree of product removal increased with the increase in the impingement angle from 30 to 90°. The corrosion products at a flow rate of 18 l/min were identified as those of

toothed type in a porous surface (Figure 7), which is more evident for coupons at 30° and 90°; while on coupon at 60° a greater amount of deposits is observed.



**Figure 6.** Micrographs of corrosion products deposited on the metallic coupons at the impingement angles indicated and a flow rate of 18 l/min (300X). The arrows indicate flow direction.



**Figure 7.** SEM images of corrosion products deposited on the metallic coupons at the impingement angles indicated and a flow rate of 18 l/min (1500 X).

The corrosion products displayed an increase in the density of agglomerates as the impact angle was increased from 30° to 90°. In the three surfaces, the growth of corrosion products developed in layers; this behavior can be better observed in the coupon at 90°. The removal of corrosion products is not only consequence of friction due to flow rate on the metallic surface but also it has to do with the nature of chemical species deposited, which are more or less susceptible to cracking and dissolution depending on its composition and film properties [44].

### 3.3.2 SEM characterization at a flow rate of 18 l/min with inhibitor

Figure 8 shows the metallic coupon surfaces after the addition of CI, where it is observed an increase in the density of corrosion products with the impingement angle, which was more evident on the surfaces at 30° and 90°. The effect of inhibitor is to produce a new film on the corrosion products after its adsorption process has occurred [45]. CI is capable of modifying the corrosion products morphology on formation along with its chemical composition in order to improve corrosion resistance by film modification [46].

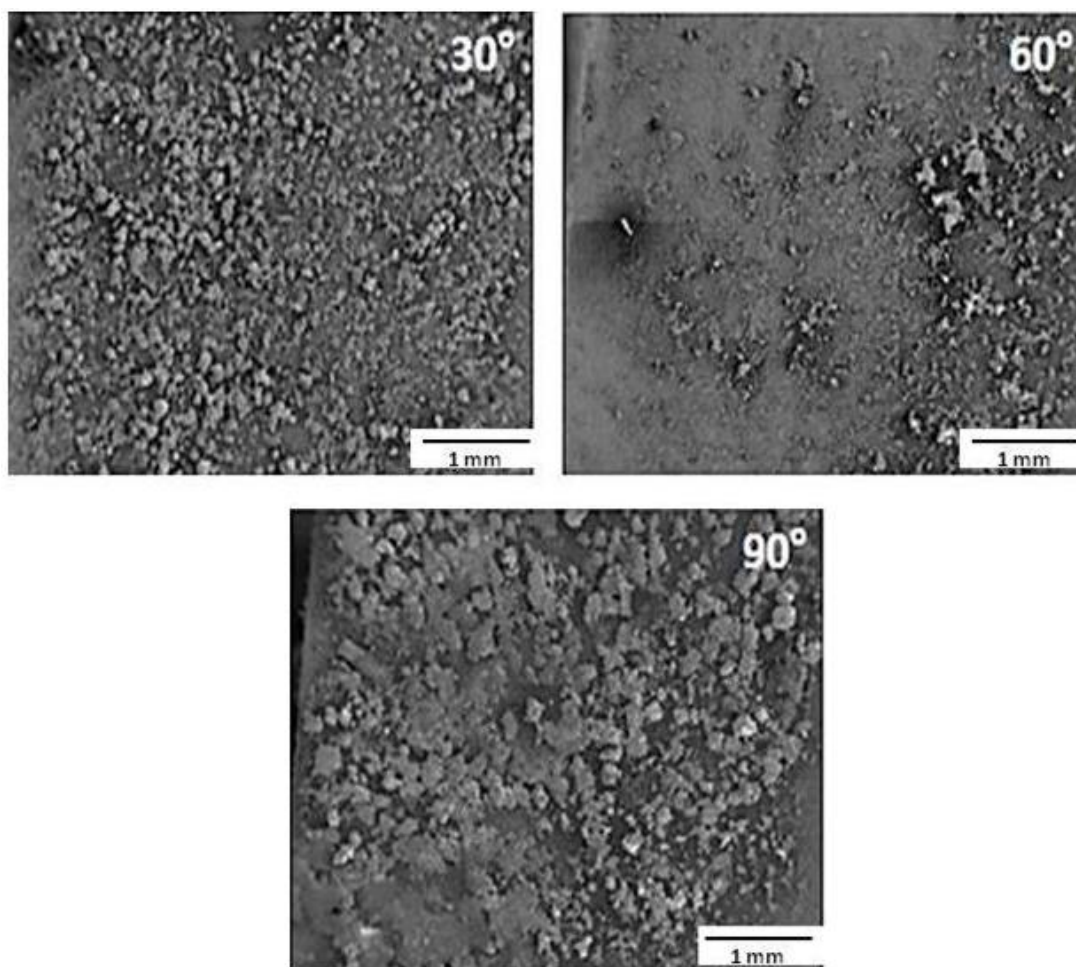


**Figure 8.** SEM images of API 5L X-70 steel coupons placed at the angles of a) 30°, b) 60° c) 90° tested at 18 l/min for 8 h in a sour brine after the addition of corrosion inhibitor (300 X).

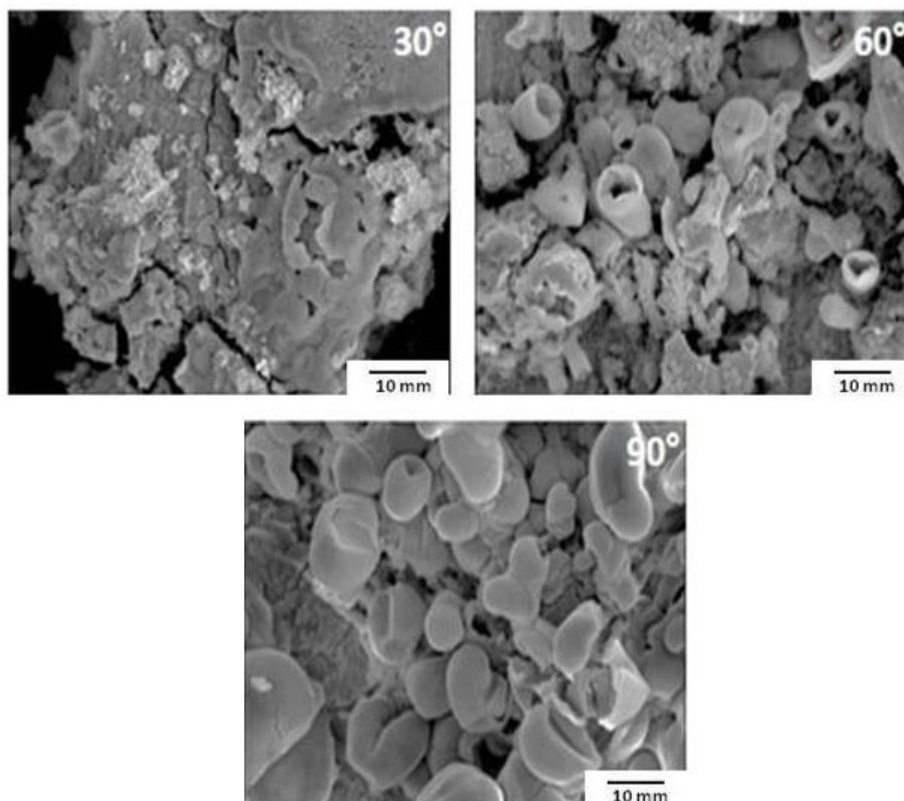


**Figure 9.** SEM images of API 5L X-70 steel coupons placed at the angles of a) 30°, b) 60° c) 90° and tested at 18 l/min for 8 h in a sour brine with inhibitor (1500 X).

This behavior is observed in more detail at higher magnifications (Figure 9), where it is observed that the serrated surfaces shown in Figure 7 were transformed into a rounded microstructure denominated of the rosebud type [47]. The corrosion products deposited on the metallic surface appears to produce a lower turbulence and in consequence FAC is mitigated. The distribution of the corrosion products seems more homogeneous than that formed in a toothed type surface without inhibitor, which means rounded deposits and lower interactions to produce micro-turbulence on steel surface [48] and in consequence deposits formed a more resistant film that might hamper the contact of steel surface with the liquid phase, which results in a lower corrosion rate.

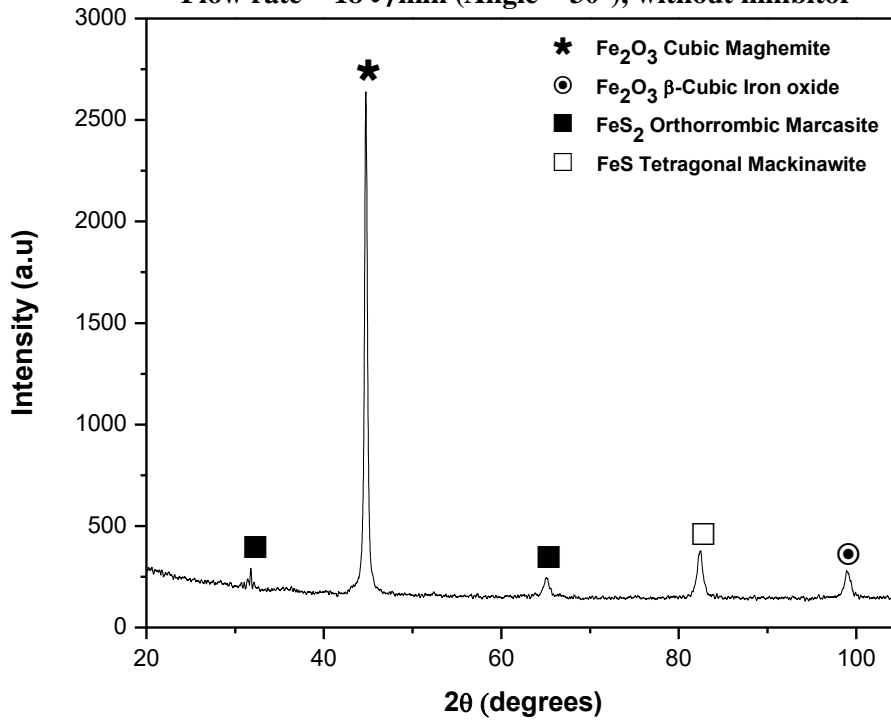
### 3.4 Characterization of corrosion products by XRD

Figure 10 shows the chemical species that appeared in the diffraction patterns at a flow rate of 18 l/min in absence of inhibitor. They are the same for the three angles of impingement: Cubic maghemite ( $\text{Fe}_2\text{O}_3$ ) as the predominant phase, tetragonal mackinawite ( $\text{FeS}$ ), orthorhombic marcasite ( $\text{FeS}_2$ ) and  $\beta$ -cubic iron oxide ( $\text{Fe}_2\text{O}_3$ ). Cubic maghemite decreased as the angle increased (30°- 90°), as it happened with  $\beta$ -cubic iron oxide, while marcasite displayed two peaks (30°, 60°) though only one at 90°. In the absence of inhibitor, the corrosion products formed are the same for the angles tested, with the feature that oxides predominated over sulfides. The presence of marcasite is known to

decrease corrosion rate owed to the crystal lattice adherence on steel surface [49], which coincides with a decrease in corrosion rate for the sample tested at 90°.

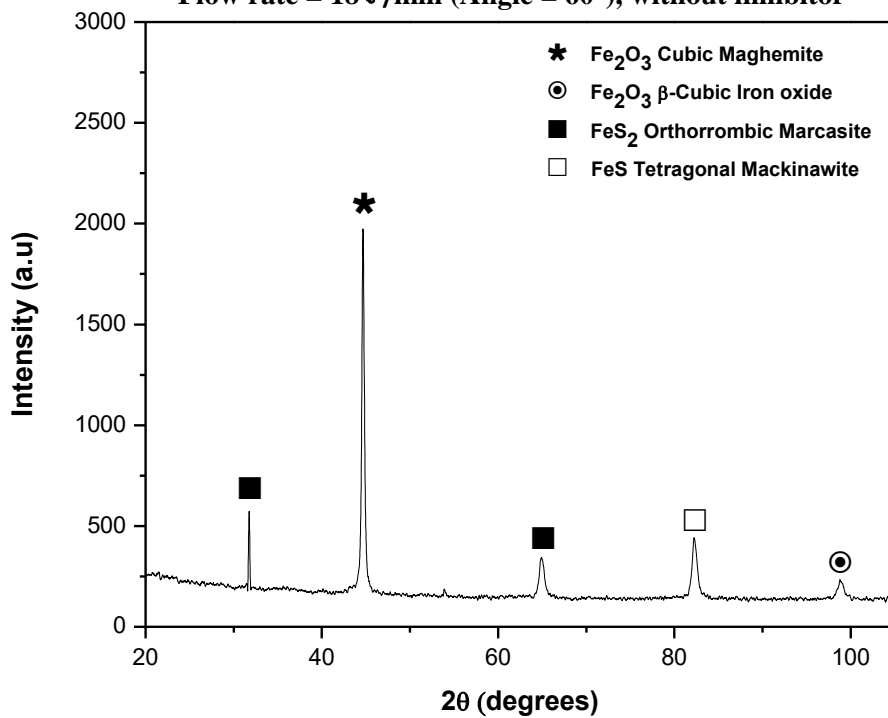
**(a) API 5L X70 Brine + 10% kerosene + 1382.7 ppm H<sub>2</sub>S**

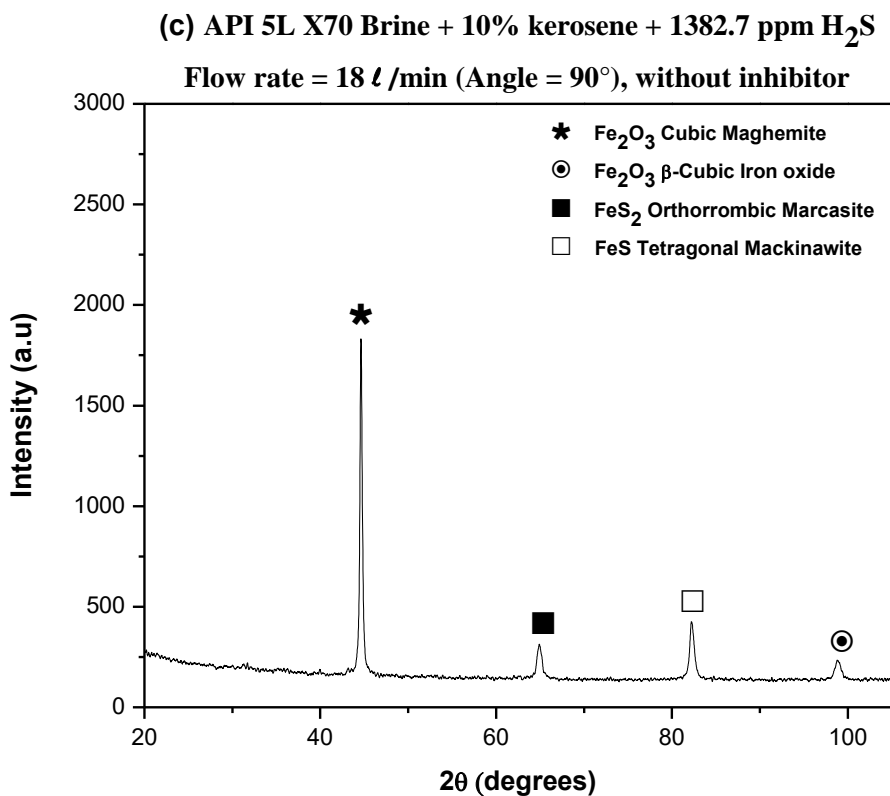
**Flow rate = 18 l/min (Angle = 30°), without inhibitor**



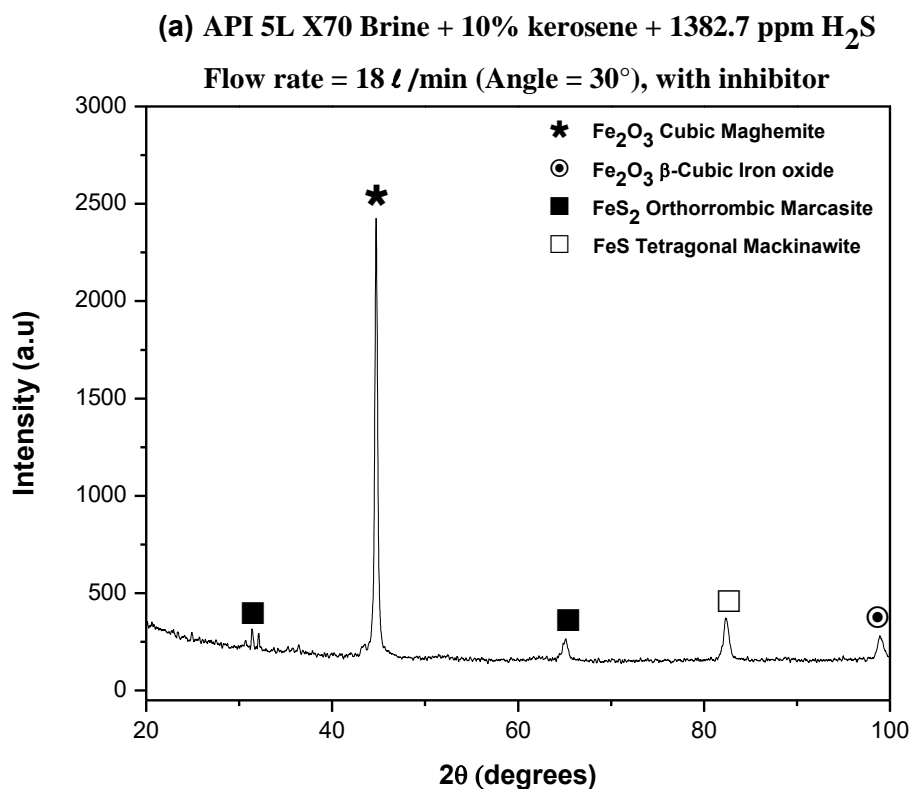
**(b) API 5L X70 Brine + 10% kerosene + 1382.7 ppm H<sub>2</sub>S**

**Flow rate = 18 l/min (Angle = 60°), without inhibitor**





**Figure 10.** XRD of corrosion products deposited on API 5L X-70 at a flow rate of 18 l/min in sour brine without inhibitor at (a) 30°, (b) 60° and (c) 90°.



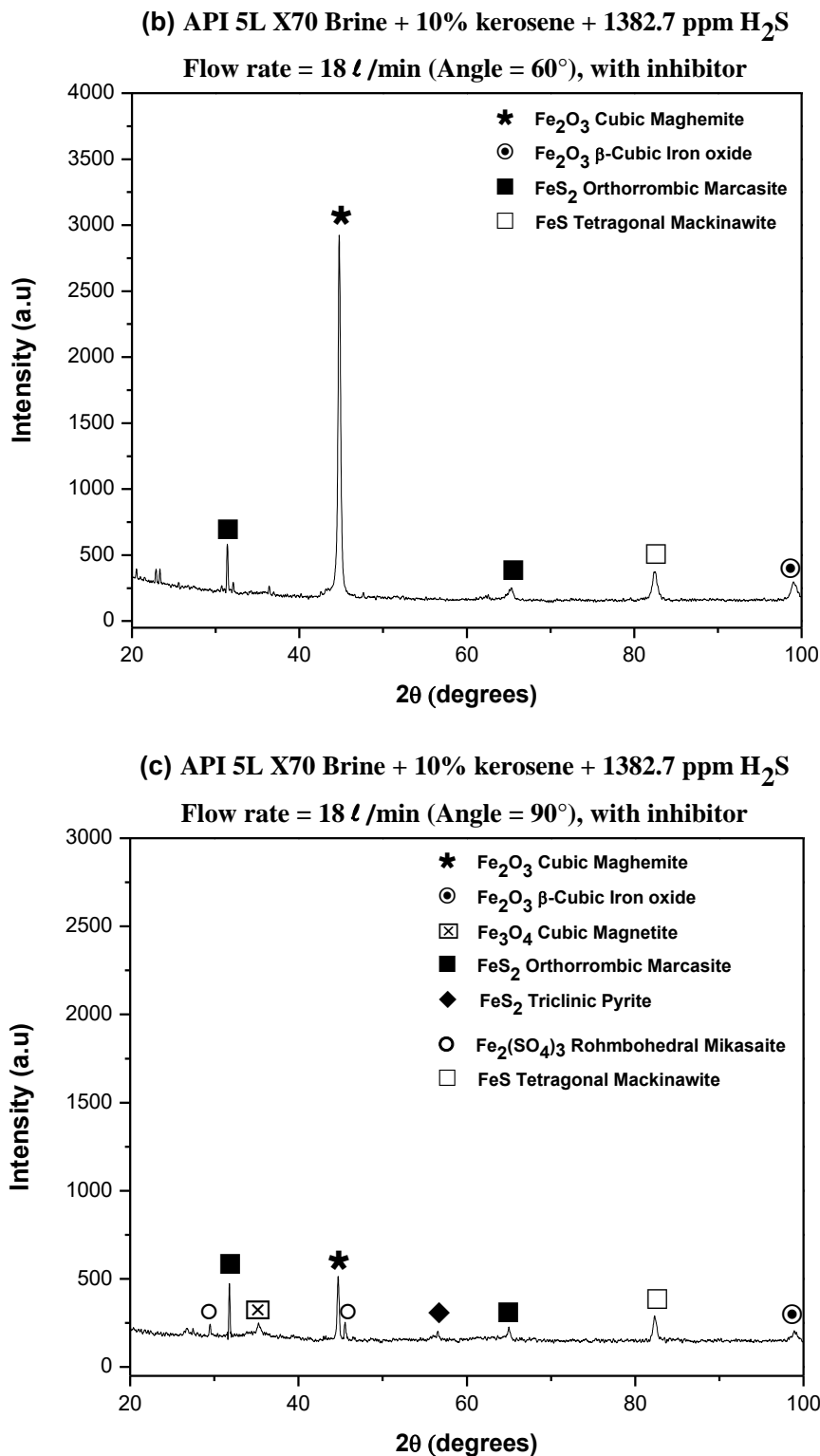


**Figure 11.** XRD analysis of corrosion products deposited on API 5L X-70 in sour brine at a flow rate of 18 L/min with inhibitor at (a) 30°, (b) 60° and (c) 90°.

Mackinawite (Fe<sub>(1-x)</sub>S) is the predominant chemical species that appeared in acid, neutral and alkaline aqueous environments below 100 °C, as a crystalline precipitate of ferrous ions in H<sub>2</sub>S [50-52]. It appears almost immediately after carbon steel immersion in aqueous solution [53].

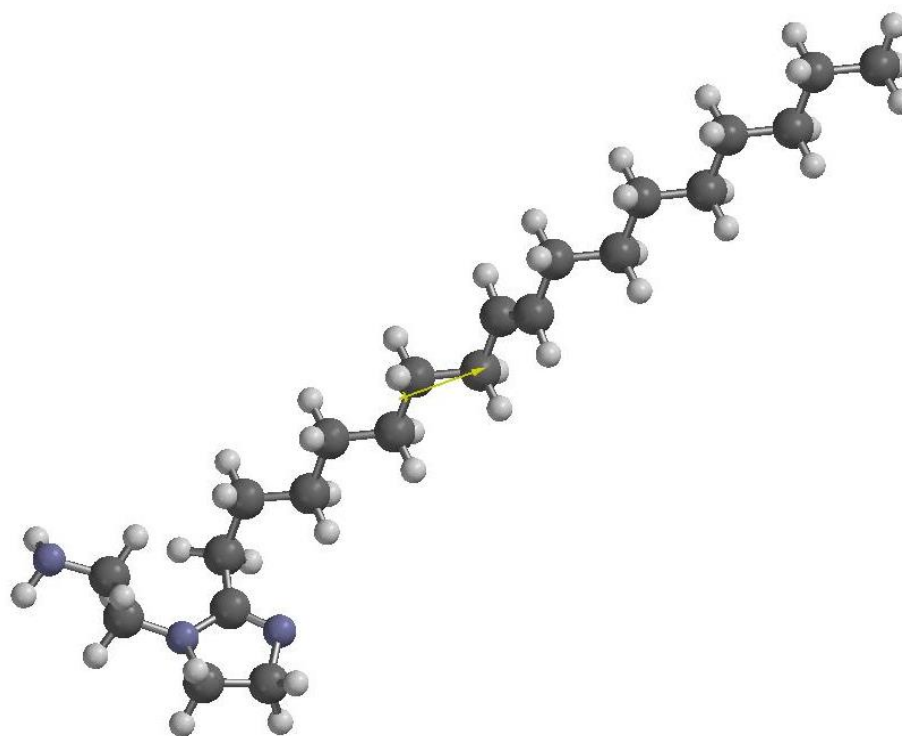
At intermediate concentrations of  $\text{H}_2\text{S}$ , mackinawite accelerates corrosion though after longer exposure times, it is converted to pyrite (cubic  $\text{FeS}_2$ ), pyrrhotite ( $\text{FeS}_{(1+x)}$ ) and troilite ( $\text{FeS}$ ) [54]. These species of iron disulfides such as pyrite and marcasite have a composition of  $\text{FeS}_{2.0}$  and it has been shown [55] that pyrite is the sole ultimate product of aqueous  $\text{H}_2\text{S}$  with iron, carbon steel, troilite and mackinawite at 100-160 °C in the absence of oxidants other than  $\text{H}_2\text{S}$ . However, in the presence of oxygen or sulfur, or under the application of anodic current at the crystallization site, marcasite is formed in addition to pyrite [56]. Troilite appears to have a higher crystalline order so seems more stable than other phases. Oxides species such as magnetite ( $\text{Fe}_3\text{O}_4$ ) and maghemite ( $\text{Fe}_2\text{O}_3$ ) are believed to be part of the inner film and those species of sulfides conformed the external layer of steel iron surface. The kinetics of pyrite and marcasite formation is slow and formation may take several days [57]. On rotating carbon steel discs in aqueous hydrogen sulfide, the evolution of corrosion products in oxygen free solutions is as follows: Mackinawite (tetragonal  $\text{FeS}_{(1-x)}$ ), ferrous sulfide (cubic  $\text{FeS}$ ), troilite (hexagonal  $\text{FeS}$ ), pyrrhotite (hexagonal  $\text{Fe}_{(1-x)}\text{S}$ ) and pyrite (cubic  $\text{FeS}_2$ ). Temperature above 100°C accelerates sequence of transformation, while higher rotational rates retard it [58].

Figure 11 shows the chemical species formed on the outer film of the steel surface at a flow rate of 18 l/min in the presence of inhibitor. Film consisted of a mixture of oxides and sulfides; at 30°/60° cubic maghemite ( $\text{Fe}_2\text{O}_3$ ) appeared as the predominant chemical specie followed by orthorhombic marcasite ( $\text{FeS}_2$ ), tetragonal mackinawite ( $\text{FeS}$ ) and  $\beta$ -cubic iron oxide ( $\text{Fe}_2\text{O}_3$ ). However, at 90°, cubic magnetite ( $\text{Fe}_3\text{O}_4$ ), triclinic pyrite ( $\text{FeS}_2$ ) and rhombohedral mikasaite ( $\text{Fe}_2(\text{SO}_4)_3$ ) appeared in addition to those at 30° and 60°. The range of the corrosion products were similar for 30° and 60°; however at 90°, the number of chemical species increased from 4 to 9, where an oxide ( $\text{Fe}_2\text{O}_3$ ) and a sulfide ( $\text{FeS}_2$ ) were the prevalent phases besides rhombohedral mikasaite is added [59].

Chemical species for the samples tested at 90° displayed some particular features in the presence and absence of inhibitor so it behaved differently to those at angles of 30-60°. In the absence of CI, corrosion products showed the lowest number of chemical species (4), in which a decrease in orthorhombic marcasite ( $\text{FeS}_2$ ) was detected. In the presence of CI, the number of chemical species increased (9), where oxides and sulfides seem to have a similar distribution. However, the film formed cannot control corrosion as it is showed by the high final corrosion rates. A plausible explanation has to do with the stagnation region where flow rate impinged at maximum rate avoiding the formation of a continuous film of inhibitor so corrosion is enhanced and inhibitor efficiency is decreased.

### 3.5 Quantum chemical calculations

After geometry optimization at level B3LYP/6-31G\*, which provides d functions to 2<sup>nd</sup> row elements (C, N, O, etc.) allowed a high reliability of simulation results (Figure 12). A total energy of  $E = 1028.48$  au along with  $E_{\text{HOMO}} = -5.26$  eV and  $E_{\text{LUMO}} = 0.96$  eV shows a high  $\Delta E = 4.3$ , which is sufficiently large to assure a strong interaction with metal substrate.



**Figure 12.** Optimized geometry of imidazoline derivative showing amine (pendant group), imidazoline (head) and alkylic chain of CI

The analysis of Mulliken's charges permits to identify the sites of inhibitor adsorption on substrate; they are indicated for the atoms involved (Table 4). The sites of ionic reactivity can be estimated from the net charges on a molecule.

**Table 4.** Mulliken's charges of selected atoms for imidazoline molecular structure.

Atom	Charge
N1	-0.453
C2	-0.144
C3	-0.163
N4	-0.484
C5	0.508
C6	-0.158
C7	-0.155
N8	-0.701
C9	-0.337

The rest of atoms in the alkylic chain are within -0.25 to -0.26 for C  $sp^3$ ; -0.3 for C  $sp^3$  adjacent to C  $sp^2$  and -0.093 for carbons C  $sp^2$ . The other hydrogen atoms are in the range of 0.11 a 0.22.

In terms of local FMO, HOMO contributions are located at N1 and N4 of imidazoline heterocyclic ring and N8 in ethylenamine moiety; meanwhile LUMO contributions are mainly located at C5-N4 in imidazoline ring and C16-C17 double bond. In Figure 13, both contributions are shown graphically.

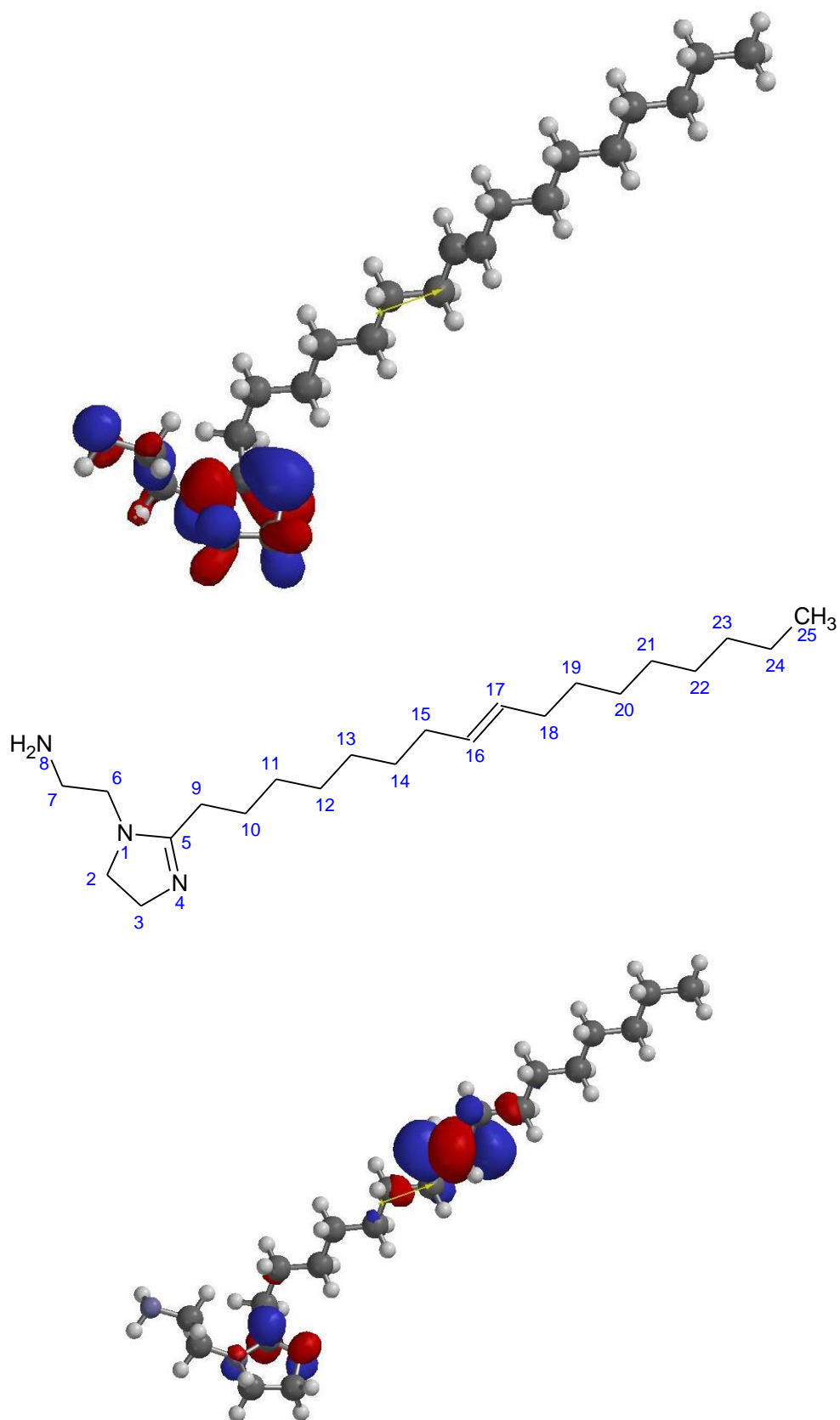


**Figure 13.** HOMO (highest occupied molecular orbital) and LUMO (lowest unoccupied molecular orbital) for CI.

In terms of global parameters, such as Pearson theory [60] hardness ( $\eta$ ) and softness ( $\sigma$ ) calculated from FMO values, imidazoline has  $\eta = (E_{\text{LUMO}} - E_{\text{HOMO}})/2 = 3.11$  eV and  $\sigma = 1/\eta = 0.322$  eV. Large values of  $\sigma$  indicate better adsorption on the metal surface [61].

#### 4. CONCLUSIONS

Inhibitor film provided efficiencies in the range of 70-99% at 200 ppm with initial corrosion rates in the range of 125-134 mpy (3.2-3.4 mm/y). In the absence of inhibitor, chemical species of cubic maghemite ( $\text{Fe}_2\text{O}_3$ ) predominated with an apparent decrease in orthorhombic marcasite ( $\text{FeS}_2$ ) when angle was increased from  $30^\circ$  to  $90^\circ$ . In the presence of inhibitor, maghemite ( $\text{Fe}_2\text{O}_3$ ) and marcasite ( $\text{FeS}_2$ ) prevailed as a mixture of oxides and sulfides at the impingement angles. Mackinawite appeared with and without the presence of corrosion inhibitor at every angle tested on the metallic surface. At  $90^\circ$ , four chemical species were detected without inhibitor, whereas nine chemical species formed in the presence of inhibitor. At  $90^\circ$ , the additions of CI did not work after 4 hours probably because of the difficulty in forming a continuous protective film on the surface directly below the stagnation region, where normal stress is at peak and corrosion rates are in the range of 90 mpy.

As the flow rate and angle were increased the inhibitor efficiency decreased due to partial film formation; imidazoline derivative is efficient under turbulent flow ( $\text{Re} = 12,500$ ) albeit a periodic replenishment is required after a 3-4 hour period.

DFT simulation of imidazoline derivative emphasized high polarity of nitrogen atoms in imidazoline and in primary amine. Likewise, its high value of energy change related to molecular orbitals (4.3 eV) indicates a relatively high capability of forming compounds, as compared, for example to benzimidazoles that may reach a value of  $\sim 5.5$  eV. Nevertheless, the molecular interactions of carbon steel with the chemical species formed under FAC conditions should be calculated along with others such as steric hindrance and non-covalent interactions.

#### ACKNOWLEDGEMENTS

The authors would like to thank the Instituto Politécnico Nacional (IPN) for the facilities provided. Acknowledgments are also due to the Instituto Mexicano del Petróleo (IMP) and the Consejo Nacional de Ciencia y Tecnología (CONACYT) for partial sponsorship.

#### References

1. R. B. Dooley, *P.P. Chem.*, 10 (2008) 68.
2. D.H. Lister and R.C. Lang, Report INIS-FR-15-66 (2001).
3. T.M. Laronge and M.A. Ward, NACE International Conference 1999, paper 345.
4. R.B. Dooley and V.X. Chexal, NACE International Conference 1999, paper 347.
5. B. Poulson, 13th International conference on environmental degradation of materials in nuclear power systems (2007).
6. S. Uchida, M. Naitoh, Y. Uehara, H. Okada, S. Koshizuka and D.H. Lister, NACE International Conference 2009, paper No. 09468.
7. P.P. Bai, S. Zheng, H. Zhao, Y. Ding, J. Wu and Ch. Cheng, *Corros. Sci.* 87 (2014) 397.

8. S. Uchida, M. Naitoh, Y. Uehara, H. Okada, N. Hiranuma, W. Sugino, S. Koshizuka and D.H. Lister, *J. Nuc. Sci. Tech.*, 46 (2009) 31.
9. Y.S. Garud, M.J. Cohn, P.M. Besuner, NACE International, Jan. 1999. Paper No. 353.
10. C. Hales, K.J. Stevens, P.L. Daniel, M. Zamanzadeh and A.D. Owens, *Eng. Fail. Anal.*, 9 (2002) 2353.
11. K.D. Efird, *J. Energ. Resour. Tech.*, 120 (1998) 72.
12. I. Betova, M. Bojinov and T. Saario, Research report NO VTT-R-08125-10, 19.10.2010.
13. C.M. Spinelli and L. Prandi, 7<sup>th</sup> pipeline technology conference 2012.
14. M. Heydari and M. Javidi, *Corros. Sci.*, 61 (2012) 148.
15. D. Belato Rosado, W. De Waele, D. Vanderschueren and S. Hertele, *J. Sustain. Constr. & Design*, 2013.
16. J.Y. Koo, M.J. Luton, N.V. Banguru, R.A. Petkovic, D. Fairchild, C.W. Petersen, H. Asahi, T. Hara, Y. Terada, M. Sugiyama, H. Tamehiro, Y. Komizo, S. Okaguchi, M. Hamada, A. Yamamoto and I. Takeuchi, Proceedings of 13<sup>th</sup> international offshore and polar engineering conference, Honolulu, Hawaii, USA, 2003.
17. M. A. J. Mazumder, H. A. Al-Muallem and S. A. Ali, *Corros. Sci.*, 90 (2015) 54.
18. M. A. Gough, W.H. Durnie, E.K. Auty and B. Hedges, *Corrosion* 2002, Paper No. 02301.
19. A.D. Mercer, L.L. Schrier, *Corrosion*, Vol. 2, 2nd ed., Butterworth, Sevenoaks, Kent, England, 1976, 18.
20. A. Edwards, C. Osborne, S. Webster, D. Klenerman, M. Joseph, P. Ostovar and M. Doyle, *Corros. Sci.*, 30 (1994) 315.
21. A.J. McMahon in Proc. 7<sup>th</sup> European Symposium on Corrosion Inhibitors, University of Ferrara, Italy, 1990, 1281.
22. V. Jovancevic, S. Ramachandran and P. Prince, *Corrosion* 55 (1999) 449.
23. X. Liu, S. Chen, H. Ma, G. Liu and L. Shen, *Appl. Surf. Sci.*, 253 (2006) 814.
24. M.W.S. Jawich, G.A. Oweimreen, and S.A. Ali, *Corros. Sci.*, 65 (2012) 104.
25. S. Nestic, *Corros. Sci.*, 49 (2007) 4308.
26. Y. Chen, G.R. Ruschau, G.H. Coch and M.M., NACE international conference 2004, Paper 04372.
27. A.J. McMahon, *Colloid. Surface*, 59 (1991) 187.
28. A.J. Szyrowski, *Brit. Corros. J.*, 35 (2000) 155.
29. L. Zao, H.K. Teng, Y.S. Yang and X. Tan, *Mater. Corros.* 55 (2004) 684.
30. A.S. Galvan Luis, M.A. Domínguez-Aguilar, J.L. González-Velázquez, M. Díaz-Cruz, A. Cervantes-Tobón and B. Castro-Domínguez, *Int. J. Electrochem. Sci.*, (2015) 9849.
31. Z. Jiashen and Z. Jingmao, *Corrosion* 49 (1993) 170.
32. A.J. Szyrowski, *Brit. Corros. J.*, 37 (2002) 141.
33. NACE International Publication 1D196 (1996).
34. H. Wang, D. Fell and S. Bailey, NACE international conference 2008. Paper No. 8644.
35. M. Stern and A.L. Geary, *J. Electrochem. Soc.* 104 (1957) 56. Y. Wu, W. Liu, J. Dai, X. Fan, J. Zhang, M. Lu, NACE International, *Corrosion* 2012, Paper No. 1238.
36. Y.S. Choi, S. Nestic and S. Ling, *Electrochim. Acta* 58 (2011) 1752.
37. A. D. Becke, *Phys. Rev. A*, 38, (1988) 3098.
38. Spartan '02, Wavefunction, Inc. Irvine, CA.
39. A.S. Fouda, K. Shalabi and R. Ezzat, *J. Mater. Environ. Sci.* 4 (2015) 1022.
40. S. Zhang, Z. Tao, S. Liao, F. Wu, *Corros. Sci.* 52 (2010) 3126.
41. F. Bentiss, M. Traisnel and M. Lagrenee, *J. Appl. Electrochem.* 31 (2001) 41.
42. G. Schmitt, *Mater Corros.* 52 (2001) 329.
43. E. Barmatov, T. Hughes, M. Nagl, *Corros. Sci.* 92 (2015) 85.
44. F. Shi, L. Zhang, J. Yang, M. Lu, J. Ding and H. Li, *Corros. Sci.* 102 (2016) 103.
45. P. Bai, H. Zhao, S. Zheng and Ch. Chen, *Corros. Sci.*, 93 (2015) 109.
46. K. Sapre, S. Seal, P. Jepson, H.B. Wang, Z. Rahman and T. Smith, *Corros. Sci.*, 45 (2003) 59.

47. D.B. Hmamou, R. Salghi, A. Zarrouk, R. Touzani, B. Hammouti and A.El. Assyry, *J. Environ. Chem. Eng.*, 3 (2015) 2031.
48. G.A. Schmitt, W. Bucken and R. Fanebust, *Corrosion* 48 (1992) 431.
49. J.S. Smith and J.D.A. Miller, *Brit. Corros. J.*, 10 (1975) 136.
50. D.W. Shoesmith, P. Taylor, M. Grant Bailey and D.G. Owen, *J. Electrochem. Soc.* (1980) 127 1007.
51. D.W. Shoesmith, P. Taylor, M.G. Bailey and B. Ikeda, *Electrochim. Acta* 23 (1978) 903.
52. D.W. Shoesmith, M.G. Bailey and B. Ikeda, *Electrochim. Acta* 23 (1978) 1329.
53. P. Taylor, *Am. Mineral.* 65 (1980) 1026.
54. H. Ma, X. Cheng, G. Li, S. Chen, Z. Quan, S. Zhai and L. Niu, *Corros. Sci* 42 (2000) 1669.
55. Y. Zheng, J. Ning, B. Brown, D. Young and S. Nescic, NACE international *Corrosion* 2015, Paper No. 5933.
56. S.N. Smith, NACE international, *Corrosion* 2015, Paper No. 5485.
57. F. Shi, L. Zhang, J. Yang, M. Lu, J. Ding and H. Li, *Corros. Sci.* 102 (2016) 103.
58. A.G. Wikjord, T.E. Rummery, F.E. Doem and D.G. Owen, *Corros. Sci.* 20.5 (1980), 651.
59. A. Cervantes-Tobón, M. Díaz-Cruz, J.L. González-Velázquez and J.G. Godínez-Salcedo, *Int. J. Electrochem. Sci.*, 9 (2014) 2254.
60. R.G. Pearson, *Inorg. Chem.*, 27 (1988) 734.
61. L. Fragoza Mar, O. Olivares-Xometl, M. A. Domínguez-Aguilar, E. A. Flores, P. Arellanes-Lozada and F. Jiménez-Cruz, *Corros. Sci.*, 61 (2012) 171.

© 2017 The Authors. Published by ESG ([www.electrochemsci.org](http://www.electrochemsci.org)). This article is an open access article distributed under the terms and conditions of the Creative Commons Attribution license (<http://creativecommons.org/licenses/by/4.0/>).

---